IEEE Access
Multidisciplinary | Rapid Review | Open Access Journal

Received March 24, 2019, accepted April 19, 2019, date of publication April 25, 2019, date of current version May 6, 2019.

Digital Object Identifier 10.1109/ACCESS.2019.2913181

High-Precision Measurement of Binocular Telecentric Vision System With Novel Calibration and Matching Methods

SHENGFU ZHANG[1], BO LI[1], FUJI REN[2,3], (Senior Member, IEEE), AND RONG DONG[4]

[1]School of Electronic Science and Engineering, Nanjing University, Nanjing 210046, China
[2]Department of Information Science and Intelligent Systems, Tokushima University, Tokushima 770-8501, Japan
[3]Anhui Province Key Laboratory of Affective Computing and Advanced Intelligent Machine, School of Computer and Information, Hefei University of Technology, Hefei 230602, China
[4]School of Electronics and Information, Nantong University, Nantong 226019, China

Corresponding author: Bo Li (liboee@nju.edu.cn)

This work was supported by the State Key Program of NSFC-Shenzhen Joint Foundation under Grant U1613217.

ABSTRACT In stereo vision-based three-dimensional measurements, calibration, and stereo matching are the most challenging tasks for accurate three-dimensional reconstruction. The traditional binocular vision algorithm has low precision, and we propose a binocular vision system using a telecentric lens. In this paper, we propose a calibration and matching algorithm for the telecentric binocular vision system, which collects only two pictures of the calibration plate to complete the system calibration. The algorithm is a special application of 3D reconstruction. In this paper, if the measurement points are selected as points on the grid, the appropriate extension can be used for high-precision 3D reconstruction, which will be explained in detail in the experiments. In order to reduce the calibration error and obtain high maneuverability, the binocular vision system is only calibrated once with a two-dimensional calibration board, and the depth information is obtained through the parallax of the detection process, so as to effectively simplify the calibration process and reduce the errors introduced in the calibration process. For the matching of images in the right and left cameras, the polar theory of telecentric binocular vision system is constructed according to the characteristics of telecentric lens imaging model based on the traditional binocular vision system theory. The matching algorithm only needs to apply the two-dimensional calibration information and then calculates the results according to the parallax combined with the polar line matching algorithm, which simplifies the algorithm flow and reduces the error. In this paper, experiments show that the algorithm proposed is simple and has high precision, good stability, and high-practical value.

INDEX TERMS Binocular vision, image matching, machine vision, three-dimensional sensing, calibration, image matching.

I. INTRODUCTION

With the development of image processing technology, binocular vision measurement technology has become widely used in industrial measurement processes. Machine vision measurement technology has the advantages of simple operation, no contact, high precision and low cost. Binocular vision systems mainly utilize the parallax produced by the different angles of the two cameras to obtain the three-dimensional spatial information of the object to be detected. The traditional binocular vision system detects large objects with low precision. The main reason of low accuracy of traditional binocular vision is lens perspective distortion. However, a telecentric lens has the characteristics of particularly small perspective distortion and high resolution in the depth of field; in particular, a bilateral telecentric lens can achieve less than 0.1% distortion. Compared to an ordinary industrial lens, the imaging model of a telecentric lens is parallel projection in the depth of field. If this feature of telecentric lens is applied to binocular vision systems, the effect of lens perspective on measurement accuracy can be eliminated.

In the field of computer vision, binocular vision has been studied for many decades and researchers propose a series of classical algorithms [1]–[6]. Specifically, Zuo *et al.* [7] measured 3D surfaces of complex-shaped objects to be captured with improved resolution and accuracy at up to

The associate editor coordinating the review of this manuscript and approving it for publication was Feng Shao.

10,000 fps based on their newly developed high-speed fringe projection system. Lai *et al.* [8] applied camera calibration, image preprocessing and stereo matching to calculate the distance from the camera in the actual scene. Wang *et al.* [9] studied the related difficulties and errors of binocular vision calibration and stereo matching with a large number of theoretical analyses. Guo and Liu [10] applied camera calibration, feature extraction, matching, three-dimensional reconstruction and other steps to obtain the depth of the three-dimensional scene information. Jin and Li [11] used a binocular vision system for a large-scale three-dimensional measurement system to guide welding work. A large perspective distortion arises in these applications when using ordinary cameras and lenses, so the general accuracy is relatively low. In the field of micro-vision measurement, Yan *et al.* [12] proposed an intensive fine matching algorithm and improves the matching algorithm in the binocular vision with a system detection accuracy of $\pm 1.3\%$, but this algorithm requires that the objects detected have a clear and easy extraction outline. Chen *et al.* [13], [14] proposed a telecentric binocular vision calibration algorithm, which needs to move the calibration plate in space and has complex operation. Gorpas *et al.* [15] proposed the use of a telecentric lens for the binocular micro-vision measurement of fibers in the three-dimensional space position used in a fiber alignment welding to achieve a higher accuracy, but the process used for processing is complex with high calibration error. Espino *et al.* [18] used a telecentric binocular vision system for animal tumor non-contact angiography to accurately reconstruct its three-dimensional structure, although a feature matching algorithm with low precision is applied.

The traditional binocular vision system processing algorithm is difficult to apply in the high-precision measurement field due to the impact of the lens perspective transformation and calibration complex [17], [18], [30]. [3], [16], [19] use the grid on the detection object to detect the matching points on the grid for three-dimensional reconstruction, but adopt the traditional calibration method and match according to the brightness information of the grid, which will introduce large errors in calibration and matching. This paper optimizes the calibration and matching algorithms to minimize system errors. In the field of industrial measurement, it is often necessary to measure the relative height between the production parts, such as the precise height of the wire in the production of a voice coil, to control the quality of the product [36]. In this paper, we propose the binocular stereo vision calibration, matching and distance calculation algorithm for the typical application of height measurement. This paper presents a simple, low complexity and high-precision wire-height measurement model. According to the characteristics of the telecentric camera, it is proposed that the calibration algorithm can be completed by simply taking a picture at the calibration plate. Because the telephoto lens depth of field is smaller, the calibration uses a specially designed two-dimensional plane calibration plate. Combined with the special line theory of telecentric cameraman, a line-matching algorithm is proposed to obtain a high-precision matching point pair. According to the limitation of using the two-dimensional plane calibration plate, the algorithm for calculating the height of the object to be measured according to the parameters obtained by the calibration of the two-dimensional calibration plate and the matching algorithm is proposed. The experimental results show that the algorithm has high stability and accuracy.

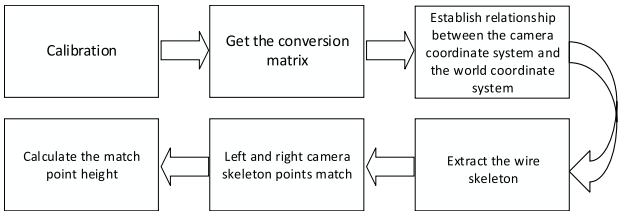

FIGURE 1. Process flow chart.

The paper is organized as follows. Section II introduces the calibration and matching algorithm. Results of the new method and comparison with existing algorithms are given in Section III. Section IV presents the discussion and conclusions.

II. PRINCIPLE OF BINOCULAR VISION MEASUREMENT

A. MODEL OF THE TELECENTRIC VISION SYSTEM

In the telecentric vision system, we choose the dual-sided telephoto lens with the smallest distortion (less than 0.1%) without a distortion correction to reduce the distortion of the telecentric lens to the measurement accuracy [19]. As shown in Figure 2, we have defined the world coordinate system $O_W(X_W, Y_W, Z_W, 1)$, the camera coordinate system $O_C(X_C, Y_C, Z_C, 1)$, and the pixel coordinate system $O_p(u, v, 1)$ [20], [32]; in this case, the pixel coordinate system and the camera coordinate system were set parallel to the projection model of the bilateral telecentric lens [21]. The coordinate origin of the pixel coordinate system is defined as the upper left of the CCD(Charge Coupled Device) array, and its coordinate value is related to the pixel arrangement value.

The difference between a telephoto lens and an ordinary industrial lens is the perspective transformation of the common industrial lens imaging model [37], [38]. The telecentricity of a telecentric lens within the depth of field is usually less than 0.1%. Specifically, a parallel projection occurs within the depth of field in a telecentric lens.

In this paper, the purpose of two-dimensional calibration is to calculate the transformation relationship between the world coordinate system and the pixel coordinate system. Because the telecentric imaging model is a parallel projection within the depth of field, the transformation from the camera coordinate system to the pixel coordinate system is accomplished by the following equation:

$$\begin{bmatrix} u \\ v \\ 1 \end{bmatrix} = \begin{bmatrix} m_{11} & m_{12} & 0 & t_u \\ m_{21} & m_{22} & 0 & t_v \\ 0 & 0 & 0 & 1 \end{bmatrix} \begin{bmatrix} \mathrm{X}_c \\ \mathrm{Y}_c \\ \mathrm{Z}_c \\ 1 \end{bmatrix} \tag{1}$$

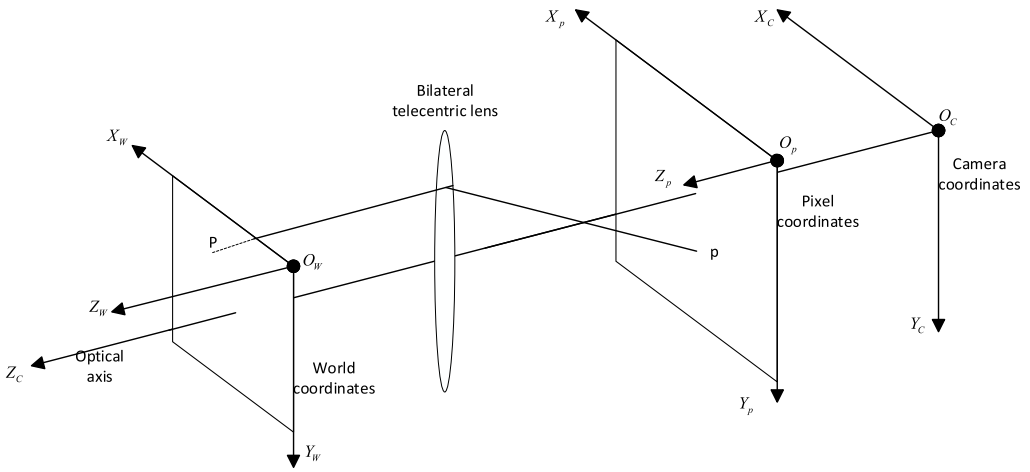

FIGURE 2. Model of the telecentric vision system.

From equation (1), equation (2) can be obtained:

$$\begin{bmatrix} u \\ v \\ 1 \end{bmatrix} = \begin{bmatrix} m_{11} & m_{12} & t_u \\ m_{21} & m_{22} & t_v \\ 0 & 0 & 1 \end{bmatrix} \begin{bmatrix} r_{11} & r_{12} & r_{13} & t_x \\ r_{21} & r_{22} & r_{23} & t_y \\ 0 & 0 & 0 & 1 \end{bmatrix} \times \begin{bmatrix} X_w \\ Y_w \\ Z_w \\ 1 \end{bmatrix} \tag{2}$$

$\mathbf{R} = \begin{bmatrix} r_{11} & r_{12} & r_{13} \\ r_{21} & r_{22} & r_{23} \end{bmatrix}$ is the rotation matrix between world coordinates and camera coordinates, and $\begin{bmatrix} t_x & t_y \end{bmatrix}^T$ is the translation matrix. $\begin{bmatrix} t_u & t_v \end{bmatrix}^T$ is translation matrix between camera coordinates and pixel coordinates.

In this paper, we use the pixel coordinates (u, v) and the $\mathbf{M}$ matrix to calculate the world coordinates of the objects in the world coordinate system. $\mathbf{M}$ is defined as follows:

$$\mathbf{M} = \begin{bmatrix} m_{11} & m_{12} & t_u \\ m_{21} & m_{22} & t_v \\ 0 & 0 & 1 \end{bmatrix} \begin{bmatrix} r_{11} & r_{12} & r_{13} & t_x \\ r_{21} & r_{22} & r_{23} & t_y \\ 0 & 0 & 0 & 1 \end{bmatrix} \tag{3}$$

B. CALIBRATION OF THE TELECENTRIC VISION SYSTEM

After obtaining the calibration board image of the left and right cameras, the calibration algorithm obtains the transformation matrix between the image coordinate sytem of the left and right cameras and the world coordinate system according to the coordinate point in the calibration board.

1) CALIBRATION OF THE TELECENTRIC VISION SYSTEM

The calibration of the telecentric vision system involves the use of a three-dimensional calibration block, usually using a calibrated cube, which is not suitable for telecentric lens system calibration because of the small depth of field of the telecentric lens; otherwise, we can also calibrate the telecentric lens system with a two-dimensional calibration plate. Chen *et al.* [13] proposed raising the calibration plate for three-dimensional space calibration; however, increasing the calibration plate will introduce errors, and the operation is inconvenient [22]. Because we need to measure the height of objects in three-dimensional space, a two-dimensional calibration plate or calibration cube should be used to obtain the $\mathbf{M}$ matrix [23].

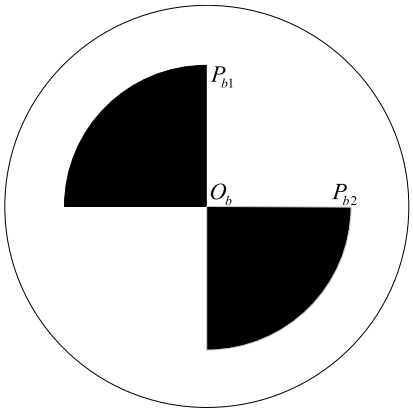

FIGURE 3. Calibration plate.

In this paper, we use the two-dimensional plane calibration plate and take two pictures of the left and right camera to complete the calibration; the calibration plate pattern is shown in Figure 3.

In Figure 3, the length of line O_bP_{b1} and the length of O_bP_{b2} is known. Line segment O_bP_{b1} is perpendicular to the line segment O_bP_{b2}, and we set the line segments O_bP_{b1} and O_bP_{b2} to Y_w and X_w for the establishment of the world coordinate system, respectively. We set the plane of the calibration plate as the reference plane, meaning that $Z_w = 0$. So we can obtain equation (4) from equation (2):

$$\begin{bmatrix} u' \\ v' \\ 1 \end{bmatrix} = \begin{bmatrix} m_{11} & m_{12} & t_u \\ m_{21} & m_{22} & t_v \\ 0 & 0 & 1 \end{bmatrix} \begin{bmatrix} r_{11} & r_{12} & t_x \\ r_{21} & r_{22} & t_y \\ 0 & 0 & 1 \end{bmatrix} \begin{bmatrix} X_w \\ Y_w \\ 1 \end{bmatrix} \tag{4}$$

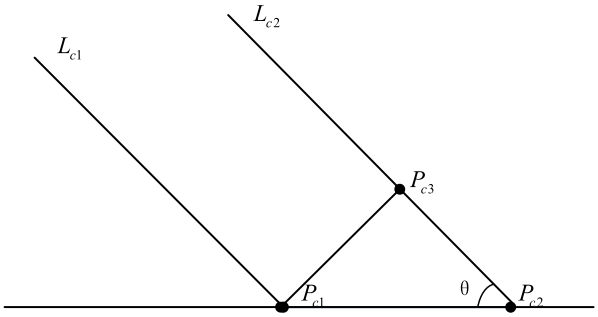

FIGURE 4. Calibration circular geometric analysis.

If

$$\mathbf{M}' = \begin{bmatrix} m_{11} & m_{12} & t_u \\ m_{21} & m_{22} & t_v \\ 0 & 0 & 1 \end{bmatrix} \begin{bmatrix} r_{11} & r_{12} & t_x \\ r_{21} & r_{22} & t_y \\ 0 & 0 & 1 \end{bmatrix}$$

and the world coordinates of O_b, P_{b1}, P_{b2} and their corresponding coordinates in the image coordinate system are known, the matrix $\mathbf{M}'$ can be obtained. Through the matrix $\mathbf{M}'$ and location in the image coordinates, the corresponding location in the world coordinates on the reference plane can also be obtained through equation (5):

$$\begin{bmatrix} X_w \\ Y_w \\ 1 \end{bmatrix} = \mathbf{M}'^{-1} \begin{bmatrix} u' \\ v' \\ 1 \end{bmatrix} \tag{5}$$

Through the above calculation, we can get the affine transformation matrix on the reference plane. The traditional way to get $\mathbf{M}$ is to move the calibration plate in the Z_w direction, but the distance traveled can not be known exactly and therefore introduces calibration error. In the following section, we obtain the three-dimensional spatial relationship of binocular vision system through the angle between the camera's optical axis and the reference plane.

2) THREE-DIMENSIONAL RELATIONSHIP

For a circle on the plane, if it is a parallel projection and the projection direction and the circular plane are not perpendicular, then the projection is elliptical. As a result, we can obtain the angle between the projection light and the plane through the ratio of the long axis to the short axis that passes through the ellipse, as shown below.

In the figure above, line segment $P_{c1}P_{c2}$ is the diameter of the circle, and L_{c1} and L_{c2} are the projection light parallel to the optical axis of the camera. Line segment $P_{c1}P_{c3}$ is perpendicular to L_{c1}. Line segment $P_{c1}P_{c2}$ is projected on the XOY plane of the camera coordinate system as line segment $P_{c1}P_{c3}$, and the angle between the optical axis of the camera and the plane of the circle is $\theta = \angle P_{c3}P_{c2}P_{c1} = \arcsin \frac{P_{c1}P_{c3}}{P_{c1}P_{c2}}$. It can be seen from parallel projection theory that the length of the diameter of the circle perpendicular to line $P_{c1}P_{c2}$ projected to the XOY plane of the camera coordinate system is still the length of the diameter. Therefore, by fitting the ellipse in the image coordinate system projected by the circle, the ratio of the short axis to the major axis of the ellipse can be used to calculate the angle of the camera relative to the reference plane.

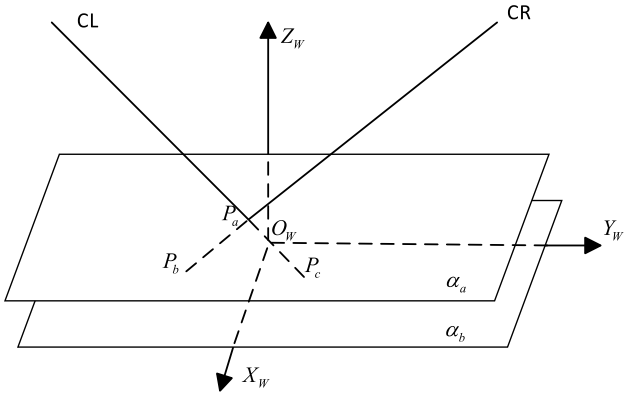

FIGURE 5. Telephoto lens visual system coordinate analysis.

The three-dimensional spatial relationship of binocular vision system is obtained by combining the affine matrix $\mathbf{M}'$ and the angle between the optical axis of the camera and the reference plane. But we don't have to calculate $\mathbf{M}$, in fact, we can use only the affine matrix and angle $\theta$to find the height of the matching point.

For the telecentric binocular vision system, the method used to calibrate the telecentric binocular vision system has been relatively complicated due to the small teleportation range of the telecentric lens [13]. This paper proposes calibration of the telecentric vision system model using the imaging of the geometric shape on the two-dimensional calibration plate. This calibration method just requires two images of the right camera and the left camera. The calibration operation is simple because we don't need to move the calibration plate in space and there is no adjustment to the calibration plate position that will introduce error into the spatial calibration.

The task of this paper is to calculate the height of the detection wire relative to the calibration plate. Therefore, in the calibration algorithm proposed in this paper, it is not necessary to calibrate the perspective transformation matrix, and only need to obtain the affine transformation matrix in the calibration plane. In the matching algorithm proposed later, the height of the measurement point can be calculated by using the projection parallax of the measurement point on the calibration plane, thereby simplifying the calibration process and improving the accuracy of the result.

C. DUAL TELEPHOTO LENS VISION SYSTEM

In Section II-B, we calibrate the system to obtain the affine matrix $\mathbf{M}'$ and the angle θ between the optical axis of the camera and the plane of the circle. This section explains how to solve the height of the match point.

As shown in Figure 5, CR is a straight line parallel to the optical axis of the right camera. The plane α_b is the plane $X_W O_W Y_W$; the plane α_a is parallel to the planeα_b; and CR is crossed at points P_a and P_b with planes α_a and α_b, respectively, so that the positions of points P_a and P_b in the image coordinate system are identical.

Because points P_a and P_b are on CR, equation (6) can be stated:

$$\begin{bmatrix} u^R_{Pa} \\ v^R_{Pa} \\ 1 \end{bmatrix} = \begin{bmatrix} u^R_{Pb} \\ v^R_{Pb} \\ 1 \end{bmatrix} \tag{6}$$

Because $Z_{Pb} = 0$, equation (7) can then be stated according to equation (5):

$$\begin{bmatrix} X_{Pb} \\ Y_{Pb} \\ 1 \end{bmatrix} = \mathbf{M'^{-1}_R} \begin{bmatrix} u^R_{Pb} \\ v^R_{Pb} \\ 1 \end{bmatrix} = \begin{bmatrix} X'_{Pa} \\ Y'_{Pa} \\ 1 \end{bmatrix} = \mathbf{M'^{-1}_R} \begin{bmatrix} u^R_{Pa} \\ v^R_{Pa} \\ 1 \end{bmatrix} \tag{7}$$

Equation (7) shows the matrix $\mathbf{M}'$ obtained by calibration, which expresses the affine transformation relationship between the calibration plate datum plane and the image coordinate system. The world coordinates are obtained for point P_b, which is the projection point of P_a in plane α_a. The plane is also determined by the parallel projection model of the telecentric vision system.

For the telecentric binocular vision system, as shown in Figure 5, CL is parallel to the left camera axis and intersects with α_a and α_b at points P_a and P_b. According to the above reasoning, the following can be stated:

$$\begin{bmatrix} X''_{Pa} \\ Y''_{Pa} \\ 1 \end{bmatrix} = \mathbf{M'^{-1}_L} \begin{bmatrix} u^L_{Pa} \\ v^L_{Pa} \\ 1 \end{bmatrix} = \begin{bmatrix} X_{Pc} \\ Y_{Pc} \\ 1 \end{bmatrix} = \mathbf{M'^{-1}_L} \begin{bmatrix} u^L_{Pc} \\ v^L_{Pc} \\ 1 \end{bmatrix} \tag{8}$$

Thus, for point P_a on plane α_a, the coordinates in the left and right camera images are converted to the calibration plate datum plane by matrix $\mathbf{M}'$, respectively, along the left and right optical axes projected onto the calibration plate reference plane.

As shown in Figure 6, points P_c and P_b on the calibration plate datum plane along the left and right optical axes projected by point P_a on plane α_a can be obtained through equations (7) and (8). Angles β_1 and β_2 between the left and right optical axes and the calibration plate reference plane have been obtained by the calibration of the camera. In Figure 6, line segment P_aP_d is perpendicular to line P_bP_c, such that equation (11) can be developed as a combination of equations (9) and (10):

$$P_bP_c = \sqrt{(X_{Pc} - X_{Pb})^2 + (Y_{Pc} - Y_{Pb})^2} \tag{9}$$

$$\tan(\beta_1) = \frac{P_aP_d}{P_bP_d}, \tan(\beta_2) = \frac{P_aP_d}{P_cP_d} \tag{10}$$

$$P_aP_d = \frac{P_bP_c * \tan(\beta_1) * \tan(\beta_2)}{\tan(\beta_1) + \tan(\beta_2)} \tag{11}$$

After determining matrix $\mathbf{M}'$ obtained using the two-dimensional calibration plate and the camera angle θ obtained using the circle in the calibration plate, matrix $\mathbf{M}$ does not need to be obtained for the height of the objects relative to the calibration plate. This method makes full use of the characteristics of the telecentric binocular vision system and successfully achieves the dimensionality of the calibration method.

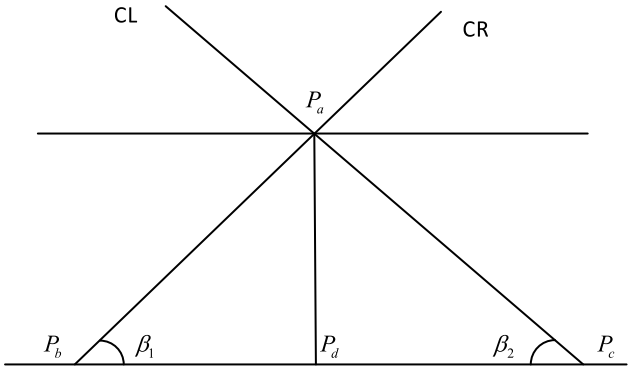

FIGURE 6. Binocular height calculation model.

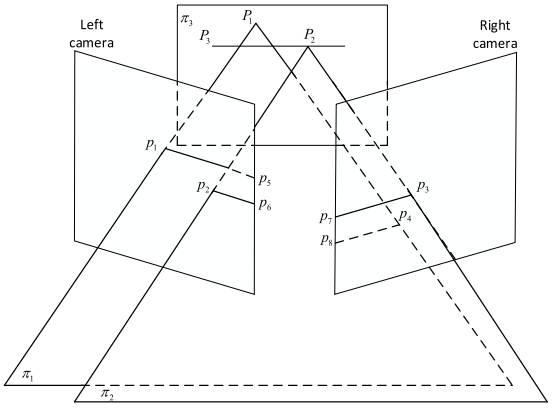

FIGURE 7. Schematic diagram of affine pole geometry.

D. BINOCULAR VISION POINT MATCHING

In Section II-C, it is assumed that P_a is the matching point. In the binocular vision system of this paper, high precision point matching and low complexity of the algorithm are very important. There has been significant research in point matching [33], and the matching error of the corresponding pixels in the traditional method is large [35], such as SIFT and SURF [24]. According to the characteristics of the telecentric imaging model, this paper presents a high-precision polar-line-matching algorithm.

Figure 7 depicts a geometric schematic of telecentric cameras. The imaging model of ordinary lens is perspective transformation. The common lens imaging model has a projection center, and a number of polar planes intersect at the baseline, but the telecentric lens imaging model is a parallel projection model. Hence, the projection center occurs at infinity, and each pole plane is parallel, so the polar lines are also parallel, and the line and the pole plane show one-to-one correspondence. This property simplifies point matching in telecentric binocular vision [25], [26]. As shown in Figure 7, π_3 is the calibration plate reference plane; the polar plane π_2 and the left and right camera coordinate planes, respectively, intersect line p_2p_6 and line p_3p_7. Point P_2 on the object in the left and right camera coordinate system corresponds to

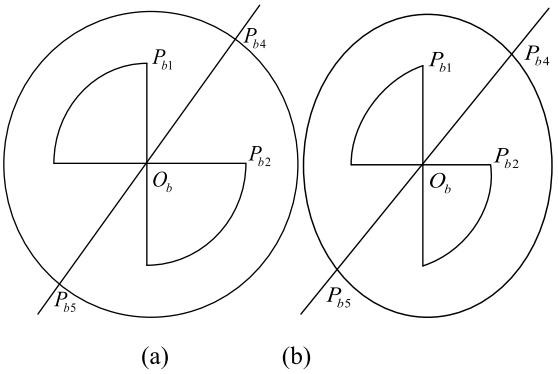

FIGURE 8. Calibration model.

points p_2 and p_3, and pole planes π_2 and π_3 intersect at line P_2P_3. Thus, the corresponding points on the left and right camera coordinate planes of the points on line P_2P_3 of plane π_3 are on p_2p_6 and p_3p_7. Because the polar planes of the telecentricity system are all parallel, the corresponding lines in plane π_3, which are parallel to line P_2P_3 in the left and right camera coordinate planes, are also parallel to lines p_2p_6 and p_3p_7. Therefore, after obtaining the corresponding relationship between lines p_2p_6 and p_3p_7 of the left and right camera coordinates, if a point p_2 is determined in the left camera, the matching point in the right camera must be on line p_3p_7 in the right camera coordinate system. Using this restriction condition, the binocular vision matching calculation is simplified; the interference of other factors is reduced; and the precision is improved.

In the ideal case, it is assumed that lines p_2P_2 and p_3P_2 in Figure 7 are a straight line parallel to the optical axis of the left and right cameras, lines p_2P_2 and p_3P_2 intersect at point P_2, and plane π_2 is perpendicular to plane π_3. As long as the position information of line p_2p_6 and line p_3p_7 can be obtained, the parallel polar line-matching algorithm can be applied to this model.

E. ANALYSIS OF POLAR LINE POSITION AND HEIGHT CALCULATION MODEL FOR THE TELECENTRIC BINOCULAR VISION SYSTEM

1) POLAR LINE POSITION

In Section II-D, we propose the telephoto binocular vision system polar line-matching algorithm, in which the accuracy of the polar line obtained is the main error of the matching algorithm. In Section II-B, we use the circle on the calibration plate to obtain the angle θ between the optical axis of the camera and the plane in which the circle resides. Through this parameter, we can determine the relative position of the camera and the calibration plate in space. The following further uses the circle on the calibration plate, and the ellipse in the image, to determine the characteristics of the line [27]–[29].

Figure 8 (a) and Figure 7 (b) show the geometric shape of the calibration plate and its geometric shape in the camera image. Because the Z-axis of the camera coordinate system is not perpendicular to the plane of the calibration plate, the circle in the calibration plate is elliptical in the image. Assuming that line $P_{b4}P_{b5}$ is a projection of a plane perpendicular to the plane of the calibration plate on the plane of the calibration plate and that the optical axis of the camera is parallel to this plane, then the projection of the optical axis of the camera on the plane of the calibration plate is parallel to line $P_{b4}P_{b5}$.

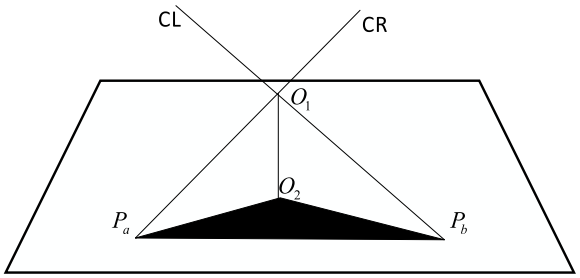

FIGURE 9. Height calculation model analysis.

In the image coordinate system, line segment $P_{b4}P_{b5}$ is the short axis of the ellipse, where we need to find the angle of line $P_{b4}P_{b5}$ and line O_bP_{b2}. Figure 8 (b) is the imaging of Figure 8 (a) in the camera coordinate system. Equation (12) is based on equation (5):

$$\begin{bmatrix} X_{Pb2} \\ Y_{Pb2} \\ 1 \end{bmatrix} = \mathbf{M'^{-1}} \begin{bmatrix} u_{Pb2'} \\ v_{Pb2'} \\ 1 \end{bmatrix}, \begin{bmatrix} X_{Ob} \\ Y_{Ob} \\ 1 \end{bmatrix} = \mathbf{M'^{-1}} \begin{bmatrix} u_{Ob'} \\ v_{Ob'} \\ 1 \end{bmatrix}$$
$$\begin{bmatrix} X_{Pb5} \\ Y_{Pb5} \\ 1 \end{bmatrix} = \mathbf{M'^{-1}} \begin{bmatrix} u_{Pb5} \\ v_{Pb5} \\ 1 \end{bmatrix} \tag{12}$$

Hence, the angle of line $P_{b4}P_{b5}$ and line O_bP_{b2} can be obtained:

$$\theta = ||\arctan(\frac{Y_{Pb5} - Y_{Ob}}{X_{Pb5} - X_{Ob}})| - |\arctan(\frac{Y_{Pb2} - Y_{Ob}}{X_{Pb2} - X_{Ob}})|| \tag{13}$$

If the angle θ of the left and right cameras is the same, the plane formed by the intersection of the lines parallel to the left and right optical axis of the camera intersects the calibration plate datum plane at line $P_{b4}P_{b5}$, such that line $P_{b4}P_{b5}$ is the polar line.

In this paper, the proposed algorithm for line matching is to make full use of the information obtained by calibration, and the processing process is simple and clear and does not introduce other errors.

2) HEIGHT CALCULATION MODEL ANALYSIS

In Section II-C, we consider the ideal height model, whereas we analyze the height calculation model under normal circumstances in this section. The height calculation model is the main source of error. In the height calculation, to simplify the calculation, some approximations are made, but the experimental results show that the accuracy of the height calculation model is still high.

Figure 9 displays the generalized height calculation model of the telecentric binocular vision system. Line O_1P_b is a straight line parallel to the optical axis of the left camera,

and line O_1P_a is a straight line parallel to the optical axis of the right camera. Because the plane formed by the axis of the two cameras is not perpendicular to the reference plate datum plane $P_aP_bO_2$, plane $P_aP_bO_1$ and plane $P_aP_bO_2$ have an angle that is not zero. Using a previous analysis, we can obtain the angle $\angle O_1\mathrm{P_b}O_2$ of line O_1P_b and plane $P_aP_bO_2$, the angle $\angle O_1\mathrm{P_a}O_2$ of line O_1P_a and plane $P_aP_bO_2$, and the angle $\angle P_aO_2P_b$ between plane $P_aP_bO_1$ and plane $P_aP_bO_2$.

According to the ideal situation in Figure 5, the calculated height $l_{O_1-P_aP_b}$ is the distance from O_1 to line segment P_aP_b in this case; hence, the relationship between $l_{O_1-P_aP_b}$ and $l_{O_1O_2}$ can be obtained through the relationship of the angle. According to the geometric relationship, $\angle O_1P_aO_2$, $\angle O_1P_bO_2$, $\angle P_aO_2P_b$ and $l_{O_1-P_aP_b}$ are already known, and O_1O_2 is perpendicular to the plane $O_2P_aP_b$. Thus, we can find the following:

$$P_aO_2 = \frac{O_1O_2}{\tan\angle O_1P_aO_2}, P_aO_1 = \frac{O_1O_2}{\sin\angle O_1P_aO_2} \tag{14}$$

$$P_bO_2 = \frac{O_1O_2}{\tan\angle O_1P_bO_2}, P_bO_1 = \frac{O_1O_2}{\sin\angle O_1P_bO_2} \tag{15}$$

$$P_aP_b = \sqrt{P_aO_2^2 + P_bO_2^2 - 2 * P_aO_2 * P_bO_2 * \cos\angle P_aO_2P_b} \tag{16}$$

$$L_{P_aO_1P_b} = \frac{1}{2}(P_aP_b + P_aO_1 + P_bO_1) \tag{17}$$

$$S_{P_aP_bO_1} = \sqrt{L_{P_aO_1P_b} * (L_{P_aO_1P_b} - P_aO_1)} * \sqrt{(L_{P_aO_1P_b} - P_bO_1) * (L_{P_aO_1P_b} - P_aP_b)} \tag{18}$$

Given the area formula, we can calculate the following:

$$l_{O_1-P_aP_b} = \frac{2 * S_{P_aP_bO_1}}{P_aP_b} \tag{19}$$

Following on the above derivation, we can obtain the relationship between $l_{O_1-P_aP_b}$ and $l_{O_1O_2}$, and it remains simple to calculate $l_{O_1-P_aP_b}$ with $l_{O_1O_2}$. However, calculating $l_{O_1O_2}$ with $l_{O_1-P_aP_b}$ by solving the quadratic equation is a complex and unstable process. To simplify the calculation, we seek to be as close as possible to an angle of 180^0 when installing a binocular vision camera in practical applications. This minimizes the difference, and the approximation can be used to avoid solving equation (19). The experimental results show that this approximation still can meet the requirements for high precision.

III. EXPERIMENTS AND DISCUSSION

The method in this paper is used to accurately measure the height of the object relative to the calibration plate reference plane. Because we need to accurately measure the height of the wire used in some industries, we do an experiment with this as an example. In the voice coil production process, manufacturers need to control the voice coil copper wire and voice coil diaphragm height difference to get a good tone.

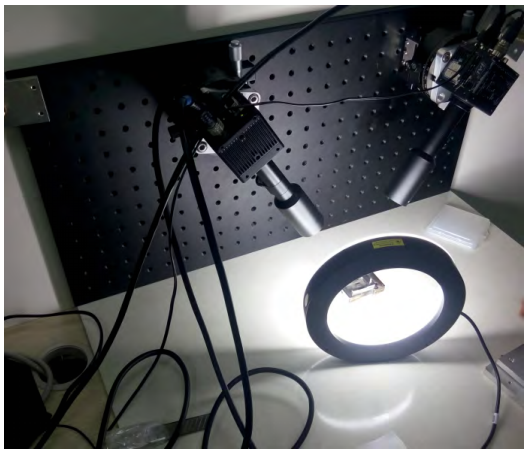

FIGURE 10. Detection system.

And we use JAI's BB500GE-S color camera with a resolution of 5 million and CanRill's XF-5MDT0.4∗110B bilateral telecentric lens. The telecentric lens used has a working distance of 110 mm, an optical distortion of less than 0.02% and a depth of field of 5.3 mm. Therefore, the lens distortion is small with no need to do distortion correction in the depth of field. In addition, we use ring light, so that the left and right cameras get the same lighting effect. The detection system is shown in Figure 10.

The 3D model of the sample is shown in Figure 11 (a), in which black is a plastic shell, yellow is a copper wire, the area of the extended single wire is the position to be detected, and blue represents the calibration plate. This article needs to detect the height of the copper wire to the blue calibration plate. Figure 11 (b) shows the detection area of different types of samples. The shape of the detection area varies with different models, but it has no effect on the application of the algorithm. The left and right camera pictures are shown in Figures 12 (a) and (b), respectively. To apply the line-matching algorithm proposed in Section II-D, it is necessary to process the wire to a line that is a single pixel wide. Because a wire is a cylinder, the width of the image in the left camera and that in the right camera is consistent throughout. In the left and right camera images, the center axis of the conductor is the skeleton of the conductor image. We first segment the image of Figures 12 (a) and (b) with a suitable threshold and then obtain the skeletal point of the copper conductor as shown in Figures 12 (c) and (d) by applying skeleton extraction as the center line of the cylindrical wire in the left and right cameras. It can be assumed that the single-pixel-wide line of Figures 12 (c) and (d) corresponds to the same line in the physical space.

Figure 13 is a photograph of the same calibration plate obtained by photographing with the left and right cameras. We establish the world coordinate system with point O_b as the origin coordinates, where the world coordinates of points O_b, P_{b1} and P_{b2} are (0, 0), (0, 1.5) and (1.5, 0) in millimeters,

TABLE 1. Data measurement.

Note: Left camera calibration points [1484.29, 628.571], [1474.29, 972.857], [1347.14, 792.857], right camera calibration points [1954.29, 625.714], [1945.71, 967.143], [1811.43, 790], relationship matrix M_{LR} =[0.9538564281753051,-0.005342564893248293, -376.4793551401976; 0.009909198622936296, 1.008617068534098, -21.90011208591243]. The angle between the left camera and the calibration plate plane is 49.5501 degrees, and the angle between the right camera and the calibration plate plane is 52.659 degrees. Because the height of a segment of the wire is measured, 10 points are averaged in the measurement area. Unit: mm.

Height	Point1	Point2	Point3	Point4	Point5	Point6	Point7	Point8	Point9	Point10	Mean
1	1.35511	1.35496	1.35481	1.35466	1.34781	1.34766	1.34081	1.34768	1.34753	1.34738	1.349841
2	1.76382	1.7637	1.76359	1.76347	1.76336	1.76325	1.75641	1.76335	1.76323	1.75639	1.762057
3	2.14961	2.14945	2.1493	2.14919	2.14908	2.14226	2.14918	2.1491	2.14899	2.14217	2.147833
4	2.5492	2.54236	2.54225	2.54217	2.54206	2.54227	2.54216	2.54204	2.54193	2.54182	2.542826
5	2.95181	2.95839	2.95151	2.95136	2.9512	2.95105	2.94417	2.93729	2.94387	2.94404	2.948469

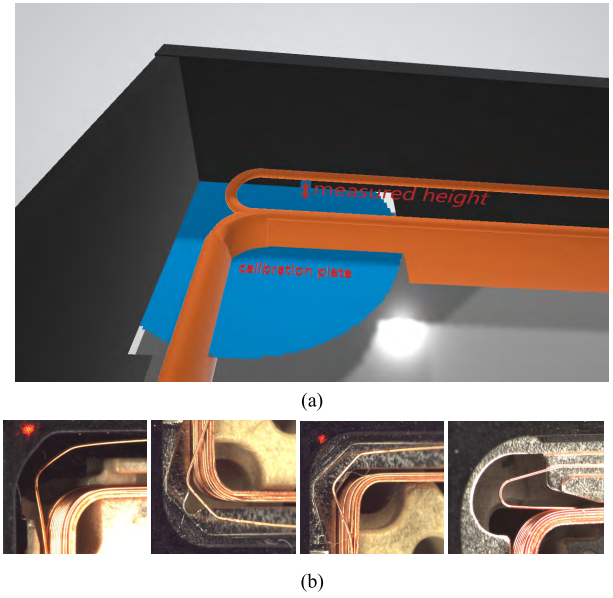

(a)

(b)

FIGURE 11. Specimen.

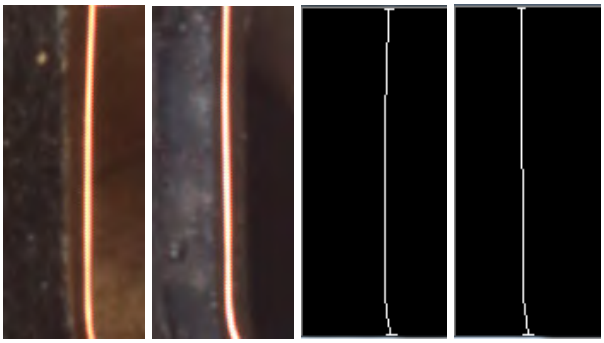

(a) (b) (c) (d)

FIGURE 12. Wire.

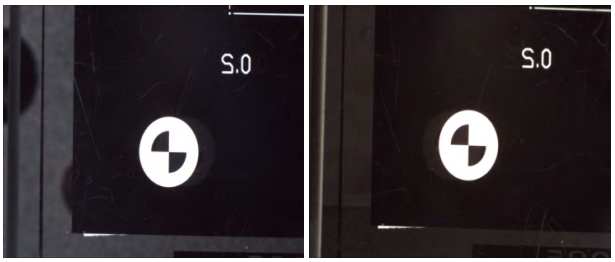

FIGURE 13. Calibration plate.

respectively. Concurrently, the relationship matrix M_{LR} of the left and right image coordinate systems is established according to O_b, P_{b1} and P_{b2}.

In the experiment, to verify the accuracy of the algorithm, we use the precision displacement table. First, we calibrate the binocular vision system in the precision displacement table as the origin, and this plane is taken as the height of the reference plane. Then, we put the sample in the precision displacement table to take pictures with the precision displacement for each increase of 0.04 mm.

A set of data measured in the test is shown in Table 1 and Table 2. In Table 1, we take 10 points at equal intervals and calculate their average. The difference between adjacent heights is 0.04 mm. In Table 2, we calculate the measurement error between adjacent mean heights. And the adjacent height difference error is not cumulative.

The traditional method of detecting measurement accuracy is to calculate the difference between the height and the absolute height of the algorithm measurement. Since the accuracy of the detection needs to be in the micrometer level, the accuracy of the algorithm is detected by the height difference. The algorithm in this paper can accurately detect the depth change in the direction of z-axis in the case of the known x-axis and y-axis coordinate positions. As shown in Figure 11 (a), the height variation of the detection point relative to the calibration plane on the micrometer level can be calculated by the calibration and matching algorithm proposed above. In this experiment, no grating is applied. By extracting the skeleton of the copper wire, the position of the physical central axis of the cylindrical copper wire is obtained, which replaces the role of the grating, so it is more accurate than the grating.

TABLE 2. Measurement error.

Height	Height 1	Height 2	Height 3	Height 4	Height 5
Mean	1.349841	1.762057	2.147833	2.542826	2.948469
Adjacent height difference	-	0.412216	0.385776	0.394943	0.405643
The actual value of adjacent height difference	-	0.04	0.04	0.04	0.04
Adjacent height difference error	-	0.012216	-0.014224	-0.005057	0.005643
Height difference error percentage	-	3.04%	-3.556%	-1.26425%	1.41075%
Height x - Height 1 (x = 2, 3, 4, 5)	-	0.41226	0.797992	1.192985	1.598628
Height x - Height 1 error	-	0.01226	-0.002008	-0.007015	-0.001372
Height x - Height 1 Percentage of error	-	3.04%	-0.251%	-0.5846%	-0.08575%

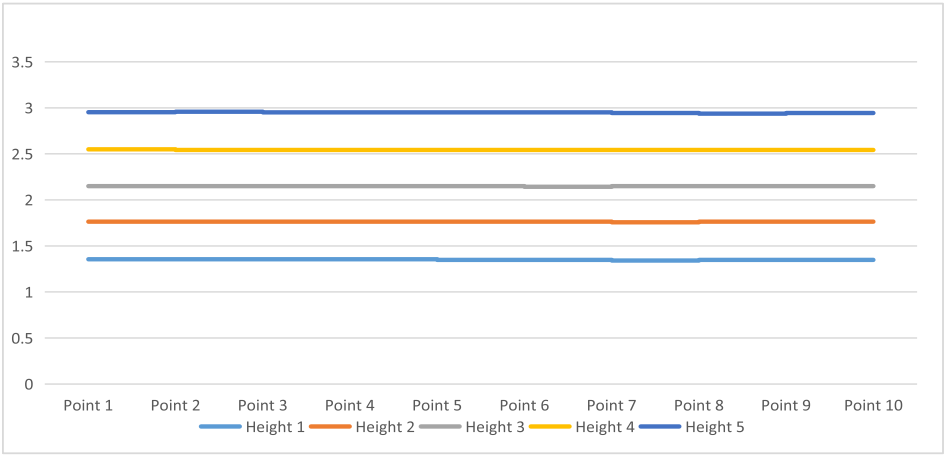

FIGURE 14. Height line chart(Unit: mm).

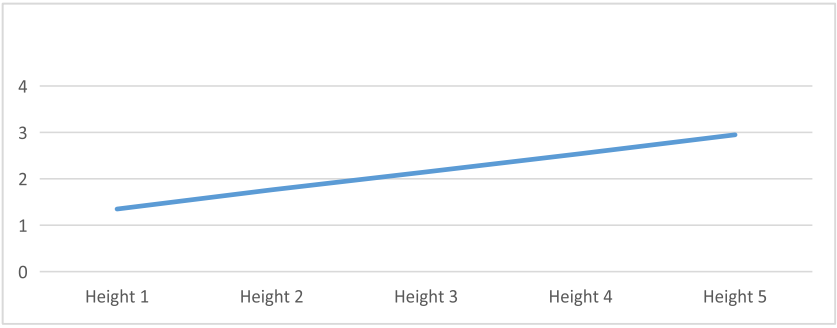

FIGURE 15. Height line chart(Unit: mm).

It can be seen from Figure 14 that the height of the measured conductor area is relatively stable, and Figure 15 shows the trend of the average height value with a linear height difference. It can be seen from Figure 14 and Figure 15 that the stability of the measurement results remains stable. From the results of the analysis in Table 2, the accuracy of the adjacent height difference is less than 4%. When the height is 0.4 mm higher than the other, the height difference is not more than 0.02 mm. We also compare the absolute height of the increase, finding that the absolute height error is even smaller and that there is no error accumulation phenomenon. The results of the above analysis show that the proposed algorithm is very stable and accurate.

The measurement errors at different camera angles are compared in Table 3. According to the error statistics in table 3, the measurement error remains stable at different angles. In practical use, the camera angle is generally adjusted between 50 and 60 degrees.

In the experiment of Figure 14, the detected wire is approximately perpendicular to the z-axis, and we have selected a section of copper wire to continuously detect its height change. The detection area of this subject cannot use gratings.

TABLE 3. Measurement error comparison of different angles.

Left camera Angle	58.8579	54.1836	49.5501
Right camera Angle	56.4132	50.6291	52.659
Height 5 - Height 1 Percentage of error	-0.04782%	-0.05164%	-0.08575%

TABLE 4. Comparation with other methods.

Method	Resolution(pixel)	RMSE	Time(ms)
Yan Hu [19]	720*540	0.0014	1361.3
Chao Zuo [3]	1024*768	0.075730	870
Ziping Liu[39]	640*480	0.037	990
Ours	2456*2058	0.02025	517.63

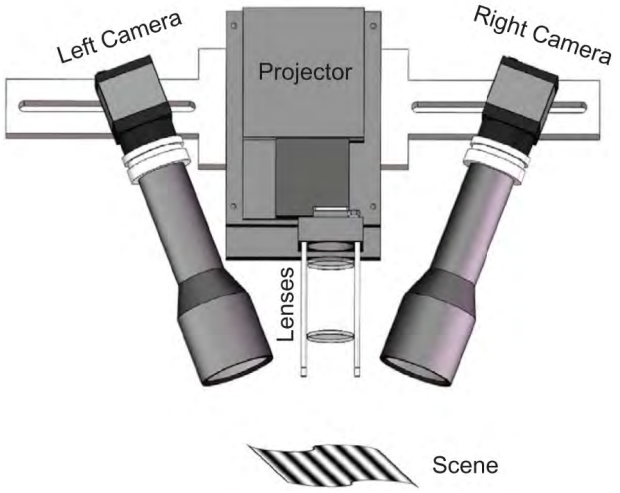

FIGURE 16. 3D reconstruction system [19].

The limitation of the algorithm for applying gratings is that the detected objects must have a certain size. The algorithm in this paper can accurately measure the information of small objects and is also a supplement to existing algorithms.

In Table 4, we compare our method to three state-of-the-art methods. These three methods are all typical algorithms for 3D reconstruction using phase shift. In the first algorithm, the author only gave the RMSE of calibration process and did not give the measurement RMSE. Ziping Liu's method gives only the standard deviation. It can be seen from Table 3 that the algorithm proposed in this paper is due to other algorithms in terms of efficiency and precision and the calibrate method is very easy to operate.

For more applications, as shown in Figure 16, this is a typical 3D reconstruction system schematic [34], using a traditional multi-space position calibration method to match the measurement points according to the brightness of the grid. Applying the algorithm of this paper, using the calibration algorithm of this paper to extract the skeleton feature points of the grid for matching, the system error in the traditional method can be reduced a lot. This is also the direction of the improvement and application of the algorithm in this paper. This paper refines the algorithm of 3D reconstruction and can be applied to more fields such as 3D reconstruction and height detection.

IV. CONCLUSION

Aiming at the complex calibration and calculation process of the current telecentric binocular vision system, this paper proposes a simple and effective calibration, matching and measurement algorithm to accurately measure its height information. In this paper, the affine transformation relationship of the system is obtained by one calibration, the parallax of different heights of the object is applied, and the height of the object is calculated by the polar line matching algorithm, which simplifies the flow of the traditional method. The experimental results show that the algorithm has high precision and stability. At the same time, the algorithm of this paper can also be extended to 3D reconstruction, which is a supplement to the existing 3D reconstruction algorithm.

REFERENCES

[1] Z. Wang, L. Zhao, and Z. Liu, "Binocular stereo vision distance measurement system based on a combination of Matlab and OpenCV," *J. Tianjin Univ. Technol.*, vol. 29, no. 1, pp. 45–48, 2013.
[2] B. Tippetts, D. J. Lee, K. Lillywhite, and J. Archibald, "Review of stereo vision algorithms and their suitability for resource-limited systems," *J. Real-Time Image Process.*, vol. 11, no. 1, pp. 5–25, 2016.
[3] C. Zuo, S. Feng, L. Huang, T. Tao, W. Yin, and Q. Chen, "Phase shifting algorithms for fringe projection profilometry: A review," *Opt. Lasers Eng.*, vol. 109, pp. 23–59, Oct. 2018.
[4] Y. Dai and K. Zhu, "A machine vision system for micro-milling tool condition monitoring," *Precis. Eng.*, vol. 52, pp. 183–191, Apr. 2018.
[5] G. Jia, X. Dong, Q. Huo, K. Wang, and X. Mei, "Positioning and navigation system based on machine vision intended for laser-electrochemical micro-hole processing," *Int. J. Adv. Manuf. Technol.*, vol. 94, nos. 1–4, pp. 1397–1410, 2018.
[6] X. Zhang, Y. Shi, B. Zhang, and C. Si, "A study of on-machine micro milling cutter condition inspection based on machine vision," *J. Micro Nano-Manuf.*, vol. 6, no. 3, 2018, Art. no. 031007.
[7] C. Zuo, T. Tao, S. Feng, L. Huang, A. Asundi, and Q. Chen, "Micro Fourier transform profilometry (μFTP): 3D shape measurement at 10,000 frames per second," *Opt. Lasers Eng.*, vol. 102, pp. 70–91, Mar. 2018.
[8] X. Lai, S. Zhu, and X. Cao, "OpenCV based camera calibration methods for seam tracking systems," *J. Welding*, vol. 31, no. 7, pp. 75–78, 2010.
[9] P. Wang, X. Han, Y. Han, and H. Qi, "The extraction of depth information about the object based on binocular vision," *Sci., Technol. Eng.*, vol. 12, no. 2, pp. 56–61, 2014.
[10] H. Guo, Y. Liu, and Y. Wang, "Calibration of binocular vision measurement of large gear workpiece welding," *J. Donghua Univ., Natural Sci.*, vol. 39, no. 4, pp. 455–459, 2013.
[11] P. Jin and F. Li, "Based on Harris corner detection algorithm," *Software*, vol. 34, no. 4, pp. 54–56, 2013.
[12] Y. Quan, S. Li, and Q. Mai, "On-machine 3D measurement of workpiece dimensions based on binocular vision," *Opt. Precis. Eng.*, vol. 21, no. 4, pp. 1054–1061, 2013.
[13] Z. Chen, H. Liao, and X. Zhang, "Telecentric stereo micro-vision system: Calibration method and experiments," *Opt. Lasers Eng.*, vol. 57, pp. 82–92, Jun. 2014.
[14] Z. Chen, D. Zhou, H. Liao, and X. Zhang, "Precision alignment of optical fibers based on telecentric stereo microvision," *IEEE/ASME Trans. Mechatronics*, vol. 21, no. 4, pp. 1924–1934, Aug. 2016.
[15] D. S. Gorpas, K. Politopoulos, and D. Yova, "Development of a computer vision binocular system for non-contact small animal model skin cancer tumour imaging," in *Proc. SPIE-Int. Soc. Opt. Eng.*, 2007, p. 6629.

[16] T. Tao, Q. Chen, J. Da, S. Feng, Y. Hu, and C. Zuo, "Real-time 3-D shape measurement with composite phase-shifting fringes and multi-view system," *Opt. Express*, vol. 24, no. 18, pp. 20253–20269, 2016.
[17] S. Zhang, "High-speed 3D shape measurement with structured light methods: A review," *Opt. Lasers Eng.*, vol. 106, pp. 119–131, Jul. 2018.
[18] J. G. R. Espino, J. J. Gonzalez-Barbosa, R. A. G. Loenzo, D. M. C. Esparza, and R. Gonzalez-Barbosa, "Vision system for 3D reconstruction with telecentric lens," in *Proc. Mex. Conf. Pattern Recognit.* Berlin, Germany: Springer, 2012, pp. 127–136.
[19] Y. Hu, Q. Chen, S. Feng, T. Tao, A. Asundi, and C. Zuo, "A new microscopic telecentric stereo vision system—Calibration, rectification, and three-dimensional reconstruction," *Opt. Lasers Eng.*, vol. 113, pp. 14–22, Feb. 2019.
[20] D. Li and J. Tian, "An accurate calibration method for a camera with telecentric lenses," *Opt. Lasers Eng.*, vol. 51, no. 5, pp. 538–541, 2013.
[21] F. Kahl, "Multiple view geometry and the L_∞-norm," in *Proc. 10th IEEE Int. Conf. Comput. Vis. (ICCV)*, Oct. 2005, pp. 1002–1009.
[22] Y. Hu, Q. Chen, T. Tao, H. Li, and C. Zuo, "Absolute three-dimensional micro surface profile measurement based on a greenough-type stereomicroscope," *Meas. Sci. Technol.*, vol. 28, no. 4, 2017, Art. no. 045004.
[23] L. Rao, F. Da, W. Kong, and H. Huang, "Flexible calibration method for telecentric fringe projection profilometry systems," *Opt. Express*, vol. 24, no. 2, pp. 1222–1237, 2016.
[24] F.-B. Wang, P. Tu, C. Wu, L. Chen, and D. Feng, "Multi-image mosaic with SIFT and vision measurement for microscale structures processed by femtosecond laser," *Opt. Lasers Eng.*, vol. 100, pp. 124–130, Jan. 2018.
[25] X. Xiao, B. Jiang, J. Ni, and C. Yan, "Research on underwater welding seam feature matching of robot binocular vision based on epipolar constraint," *Manuf. Automat.*, vol. 34, no. 10, pp. 119–123, 2012.
[26] Y. Wang, D. Xu, Y. Jiang, and C. Lu, "Study on Combined wavelet-SIFT matching and epipolar constraint algorithm for binocular stereo vision," *Comput. Technol. Develop.*, vol. 11, no. 11, pp. 81–84, 2012.
[27] Z. Xiao, W. Zhang, L. Geng, and F. Zhang, "Accuracy analysis of binocular vision system," *Optoelectron. Eng.*, vol. 41, no. 2, pp. 6–11, 2014.
[28] Q. Liu, X. Qin, S. Yin, and F. He, "Structural parameter design and accuracy analysis of binocular vision measuring system," *China Mech. Eng.*, vol. 19, no. 22, pp. 2728–2732, 2008.
[29] Y. X. Han, Z. S. Zhang, and M. Dai, "Monocular vision system for distance measurement based on feature points," *Opt. Precis. Eng.*, vol. 19, no. 5, pp. 1110–1117, 2011.
[30] J. Peng, W. Xu, and H. Yuan, "An efficient pose measurement method of a space non-cooperative target based on stereo vision," *IEEE Access*, vol. 5, pp. 22344–22362, 2017.
[31] M.-K. Kang and S.-K. Kim, "Depth perception assessment for stereoscopic 3D displays using layered random dot stereogram," *IEEE Access*, vol. 5, pp. 22855–22862, 2017.
[32] G. Xu, J. Chen, and X. Li, "3-D reconstruction of binocular vision using distance objective generated from two pairs of skew projection lines," *IEEE Access*, vol. 5, pp. 27272–27280, 2017.
[33] T. Yan, F. Zhang, Y. Mao, H. Yu, X. Qian, and R. W. H. Lau, "Depth estimation from a light field image pair with a generative model," *IEEE Access*, vol. 7, pp. 12768–12778, 2019.
[34] D. Banerjee, K. Yu, and G. Aggarwal, "Robotic arm based 3D reconstruction test automation," *IEEE Access*, vol. 6, pp. 7206–7213, 2018.
[35] X. Ye, J. Li, H. Wang, H. Huang, and X. Zhang, "Efficient stereo matching leveraging deep local and context information," *IEEE Access*, vol. 5, pp. 18745–18755, 2017.
[36] W.-C. Wang, S.-L. Chen, L.-B. Chen, and W.-J. Chang, "A machine vision based automatic optical inspection system for measuring drilling quality of printed circuit boards," *IEEE Access*, vol. 5, pp. 10817–10833, 2017.
[37] T. W. K. Poon and M. R. Friesen, "Algorithms for size and color detection of smartphone images of chronic wounds for healthcare applications," *IEEE Access*, vol. 3, pp. 1799–1808, 2015.
[38] C. Jia, F. Shi, Y. Zhao, Z. Wang, M. Zhao, and S. Chen, "Identification of pedestrians from confused planar objects using light field imaging," *IEEE Access*, vol. 6, pp. 39375–39384, 2018.
[39] Z. Liu, P. C. Zibley, and S. Zhang, "Motion-induced error compensation for phase shifting profilometry," *Opt. Express*, vol. 26, pp. 12632–12637, 2018.

SHENGFU ZHANG is currently pursuing the master's degree with Nanjing University. His research interests include image processing and machine vision.

BO LI received the Ph.D. degree, in 2009. He is currently an Associate Professor with the School of Electronic Science and Engineering, Nanjing University, where he is currently the Deputy Director of the Network Video Information Technology Research and Development Center, Zhenjiang High-Tech Research Institute. His research interests include broadband network communication, artificial intelligence, and image recognition.

FUJI REN received the Ph.D. degree from the Faculty of Engineering, Hokkaido University, Japan, in 1991. From 1991 to1994, he was a Chief Researcher with CSK. In 1994, he joined the Faculty of Information Sciences, Hiroshima City University, as an Associate Professor. Since 2001, he has been a Professor with the Faculty of Engineering, Tokushima University. His current research interests include natural language processing, artificial intelligence, affective computing, and emotional robots. He is the Academician of The Engineering Academy of Japan and the EU Academy of Sciences. He is the Editor-in-Chief of the *International Journal of Advanced Intelligence*, the Vice President of CAAI, and a Fellow of The Japan Federation of Engineering Societies, IEICE, and CAAI. He is the President of the International Advanced Information Institute, Japan.

RONG DONG received the Ph.D. degree in signal and information processing from Nanjing University, in 2012. She is currently a Lecturer with the Department of Information Engineering, School of Electronics and Information, Nantong University. Her main research interests include video image processing and machine vision.